VŠE / PRAGUE UNIVERSITY OF ECONOMICS AND BUSINESS

Article   Open Access

Deep Residual Learning Image Recognition Model for Skin Cancer Disease Detection and Classification

Jamal Mustafa Al-Tuwaijari [1] (ID)**, Naeem Th. Yousir** [2] (ID)**, Nafea Ali Majeed Alhammad** [3] (ID)**, Salama Mostafa** [4] (ID)

[1] Department of Computer Science, College of Sciences, University of Diyala, Diyala, Iraq
[2] College of Information Engineering, Al-Nahrain University, Baghdad, Iraq
[3] Department of Computer Sciences, Shatt Al-Arab University College, Basrah, Iraq
[4] Faculty of Computer Science and Information Technology, Universiti Tun Hussein Onn Malaysia, Johor, Malaysia

Corresponding author: Salama Mostafa (salama@uthm.edu.my)

Abstract

Skin cancer is undoubtedly one of the deadliest diseases, and early detection of this disease can save lives. The usefulness and capabilities of deep learning in detecting and categorizing skin cancer based on images have been investigated in many studies. However, due to the variety of skin cancer tumour shapes and colours, deep learning algorithms misclassify whether a tumour is cancerous or benign. In this paper, we employed three different pre-trained state-of-the-art deep learning models: DenseNet121, VGG19 and an improved ResNet152, in classifying a skin image dataset. The dataset has a total of 3297 dermatoscopy images and two diagnostic categories: benign and malignant. The three models are supported by transfer learning and have been tested and evaluated based on the criteria of accuracy, loss, precision, recall, f1 score and ROC. Subsequently, the results show that the improved ResNet152 model significantly outperformed the other models and achieved an accuracy score of 92% and an ROC score of 91%. The DenseNet121 and VGG19 models achieve accuracy scores of 90% and 79% and ROC scores of 88% and 75%, respectively. Subsequently, a deep residual learning skin cancer recognition (ResNetScr) system has been implemented based on the ResNet152 model, and it has the capacity to help dermatologists in diagnosing skin cancer.

Keywords

Skin cancer; Deep learning; Classification; DenseNet121; ResNet152; VGG19; Transfer learning.

1 Introduction

Skin cancer is caused by an abnormal growth of cells in the skin and is categorized as one of the deadliest types of cancer (Bellu et al., 2021). Skin cells are divided into three main types: squamous, basal and melanocytes (Valdés-Morales et al., 2020). Squamous cells are the most common form of skin cells. Melanomas are the most hazardous of the three kinds of skin cancer. It is divided again into two groups: melanocytic and nonmelanocytic (Baig et al., 2020). It is difficult to distinguish between malignant and benign melanoma. They may be mistakenly misdiagnosed and mislabelled.

Melanoma is the 19th most common cancer, and yearly cases have risen by 53 percent in recent years, with a part of the increase attributed to increasing ultraviolet (UV) radiation exposure. It is more dangerous than squamous and basal cell cancers because it spreads more quickly throughout the body (Zhu et al., 2020). As a result, proper detection or categorization of this type of skin cancer in its early stages is critical to reducing the mortality risk. To identify the malignant lesion, dermatologists would first do a visual examination of the infected region as a first stage in the diagnosis. The visual examination may often result in incorrect cancer detection, mainly when the malignancy is in its early stages. Because several lesion types are similar, it is important to get an accurate diagnosis to minimize wrong diagnoses (Dildar et al., 2021). The accuracy rate of a dermatologist was previously estimated to be between 65 and 80 percent based on visual assessment alone. Dermatologists seldom attain more than 80% of accurate diagnoses (Pérez et al., 2021).

Because of the difficulties associated with identifying skin cancer with the human eye, computer vision is used to assist in detecting skin cancer. Dermatoscopic images are collected with a specific high-resolution and magnifying camera lens in the event of a worrisome lesion, in addition to a visual examination (Tschandl et al., 2018). During the recording process, the influence of light on the image is regulated by the use of filters, which reduce reflections in the skin and, as a result, allow deeper skin layers to be seen (Valdés-Morales et al., 2020). The accuracy rate has grown tremendously due to the added technological assistance and becomes between 75 and 84 percent (Pérez et al., 2021).

Skin cancer is diagnosed and classified using either classic machine learning (ML) or deep learning (DL) techniques (Pushpalatha et al., 2021). When using a typical ML approach, a domain expert must identify the applicable characteristics and make them more clearly apparent for the learning algorithm to function, hence reducing the complexity of the problem. A DL algorithm is a subfield of ML that works with ANNs, which are algorithms inspired by the structure and function of the brain (Dildar et al., 2021). The convolutional neural network (CNN) is a standard DL model that can be trained on a large number of images, both benign and malignant (Fujisawa et al., 2019). The CNN model determines whether an image is cancerous or benign by studying the nonlinear interactions between pixels (Cassidy et al., 2022). As a result, in the DL approach, the domain knowledge is implicitly constructed during the training phase.

This research concentrates on DL using convolutional neural networks (CNN) as a base model. We contribute to improving the ResNet152 model and evaluating the performance of the model by comparing it with pre-trained DL models, namely, DenseNet121 and VGG19, in classifying the skin image dataset. The three models have been supported by a transfer learning (TL) method to pre-train the models with fine-tuned parameters. Subsequently, a deep residual learning skin cancer recognition (ResNetScr) system has been implemented in Python to assist dermatologists in diagnosing skin cancer.

This paper is organized into five sections, and the literature review is the next section. Section 3 presents the methods of the study, which include the dataset description and the DL model description. Section 4 introduces the proposed solutions and reviews the attained results. The paper ends with the conclusion section.

2   Literature Review

This section reviews the related work on skin cancer detection and classification. The review focuses on the recent modelling of CNN and the obtained test results. Yu et al. (2017) employed a CNN with feature vector encoding and a support vector machine (SVM) for classification. They avoided the issues associated with tiny datasets by providing samples or sub-images as input to the CNN rather than entire images. The suggested model was tested on 1279 skin images from the ISBI 2016 dataset. It obtained an accuracy of 83.09 percent and a receiver operating characteristic (ROC) of 73.1%.

Li et al. (2018) based their findings on the HAM10000 dataset of Tschandl et al. (2018) that is used in the ISIC 2018 challenge. They used 10,015 images and divided them into 80% for training and 20% for validation. The melanocytic nevus and tiny category included 6705 of the total number of images. Dermatofibroma was contained in 115 images, while the remainder were of melanoma and various tumour forms. They deployed various CNN models, including DenseNet201, ResNet152, Inception V4, with cropped images. The obtained results are shown in the form of a confusion matrix.

Pacheco et al. (2019) conducted a study as part of the ISIC challenge in which they utilized the same dataset we used in this work. The ISIC challenge was established to diagnose skin cancer photographs and metadata. They received the 4th place award. A total of 13 CNN models were used and compared, one of which is ResNet152. Their model obtained an accuracy of 81.8 percent, which was not the highest accuracy compared to the other models they used. The VGG-19 model achieved the highest accuracy of 84.5% compared to the other models.

In their work, Fujisawa et al. (2019) trained deep CNNs using a dataset of 4867 clinical images acquired from Tsukuba Hospital between 2003 and 2016. The dataset included 1842 images of tumours diagnosed as skin cancer and malignancies. These images depicted 14 different malignant and non-malignant tumours. The participants in this study were 13 board-certified dermatologists and nine dermatology students and residents. In the classification task, the trained CNN attained an accuracy rate of 76.5 percent, a specificity of 89.5 percent and a sensitivity of 96.3 percent.

Pushpalatha et al. (2021) have employed CNN to identify skin cancer in the ISIC dataset by masking the tumour in the skin, which they claim is a novel technique. Their approach was a little different from the others in that they utilized 90 percent of the dataset for training and 10 percent of the dataset for data augmentation, in which they rotated the images by 10 degrees and zoomed them. The model that they utilized was the industry standard Conv 2D. Their results in the segmentation were 66.35 percent, 75.10 percent and 75.50 percent for large, medium and small data shapes, respectively. Table 1 compares the previous work and our tested models based on the criteria used.

Table 1. Comparison of previous works and our work.

Ref.	Model	Accuracy	Loss	Precision	Recall	F1 score	ROC%
Yu et al. (2017)	CNN-FC6+FV	0.815	-	-	-	-	0.731
	fusion	0.830	-	-	-	-	0.795
Pacheco et al. (2019)	VGG19	0.842	-	-	-	-	0.972
	DenseNet 121	0.832	-	-	-	-	0.974
	ResNet152	0.818	-	-	-	-	0.969
Fujisawa et al. (2019)	DCNN	0.765	-	0.895	0.963	-	-
Pushpalatha et al. (2021)	DRN	0.913	0.86	-	-	-	-

3 Research Methods

To better assess the proposed ResNet152 model, we have used two other models to be compared with it, namely, VGG19 and DensNet121. The three are subjected to the same evaluation methods and dataset. This section briefly describes the dataset and the three DL models.

3.1 Dataset description

The dataset consists of skin cancer images that are taken from the ISIC archive. It is a part of the ISIC competition that was conducted in 2018 (Codella et al., 2019). Many researchers have used the ISIC archive to test different types of DL models (Cassidy et al., 2022). The images are recorded in JPEG format with a resolution of 224 x 224 pixels (Pacheco et al., 2019). The dataset comprises 3297 images of malignant (1497) and benign (1800) lesions. They are divided into training (malignant 1197 and benign 1440) and testing (malignant 300 and benign 360) sets. A dataset sample is given in Figure 1 for both benign and malignant types.
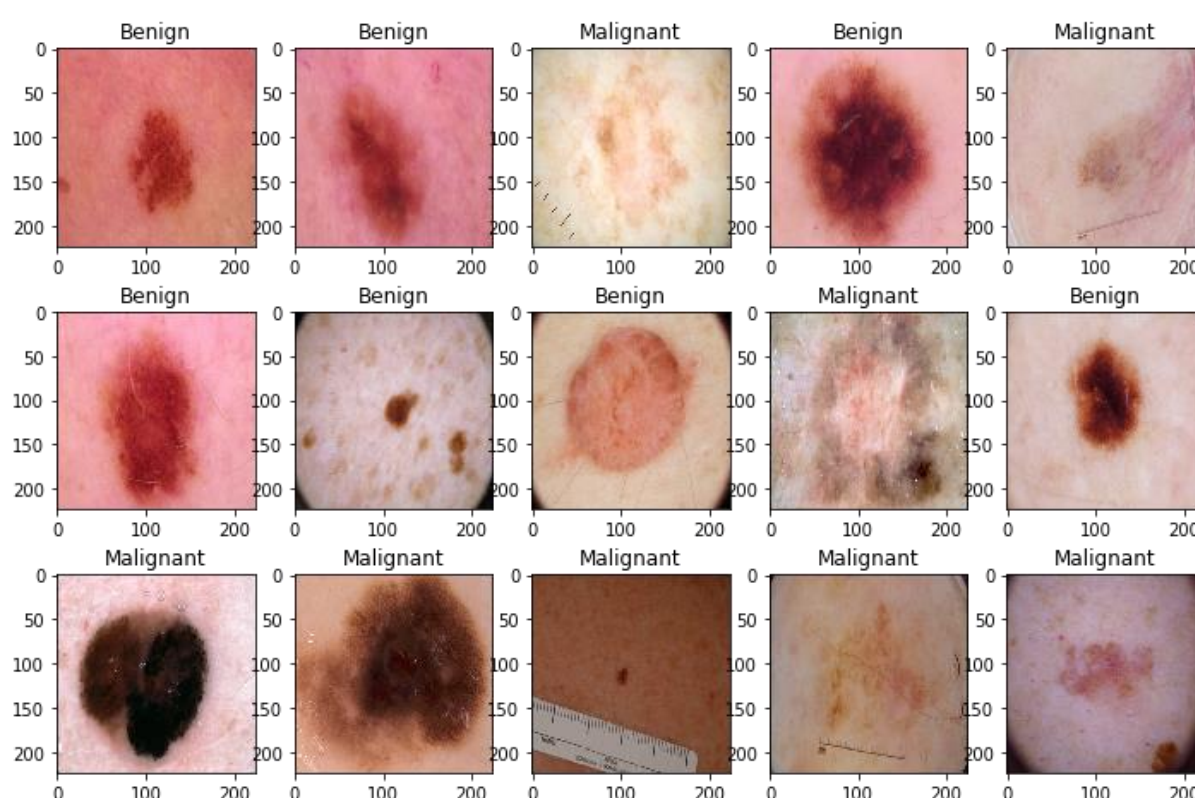

Figure 1. *Skin cancer dataset and labels.*

3.2 VGG19 model

Simonyan et al. (2014) first developed the VGG19 DL model, which is an upgraded version of the VGG16 model. Figure 2 depicts the overall design of the VGG19 model.

The VGG19 model has a deep CNN that composes of multiple convolutional layers and max-pooling layers for feature extractors. The output of each convolutional layer is calculated using the following equation.

$$y = \frac{x - k + 2*p}{s} + 1 \tag{1}$$

where y is the required output, x is the input, k is the kernel size, p is the padding and s is the stride.
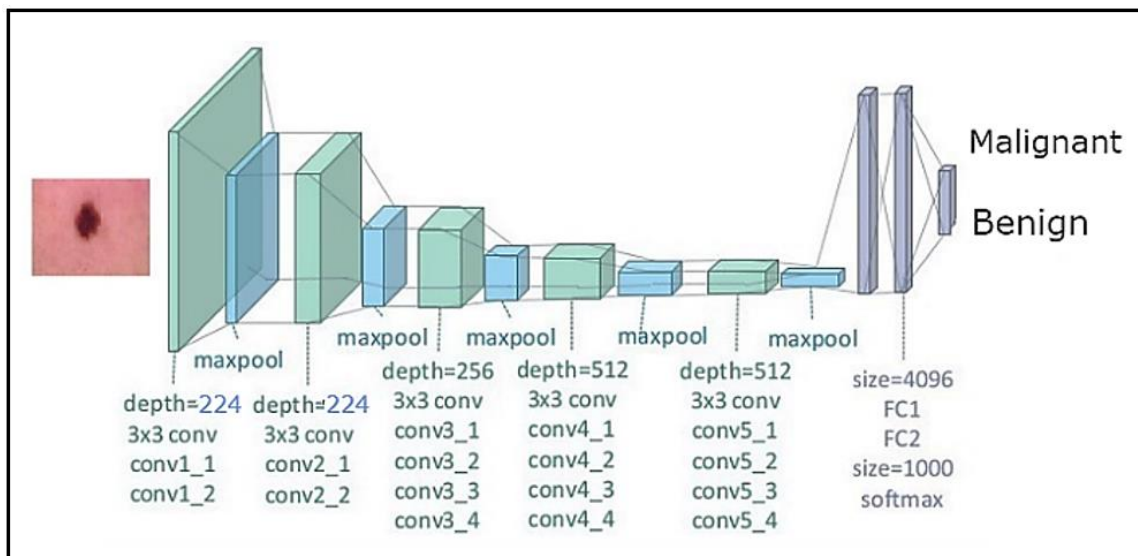
Figure 2. VGG19 architecture. Source (Zheng et al., 2018).

The max-pooling layer kernel size is also calculated based on Equation (1). Following these layers is at least one completely linked layer for classification. The size and number of the fully linked layers are not fixed and are based on the design of the CNN architecture. The hidden layers operate based on different types of activation functions, one popular of which is the sigmoid function, given in Equation (2).

$$y = \sum_{i=1}^{m}(w_i x_i) + b \tag{2}$$

where y is the output, x is the input, w is the weight and b is the bias.

3.3   DenseNet121 model

Densely connected convolutional networks, or DenseNets (Singh et al., 2021), suggest a connection design that alleviates the vanishing gradient issue that occurs during deep architecture training while ensuring maximum information and gradient flow across the network. Each layer in the DenseNet architecture is linked to the other layers in a feed-forward way, as shown in Figure 3. Each layer receives inputs from the concatenated feature maps of all previous layers and provides output to the subsequent layers. This technique can minimize the number of parameters used by reducing the number of duplicate feature mappings learned via feature reuse.
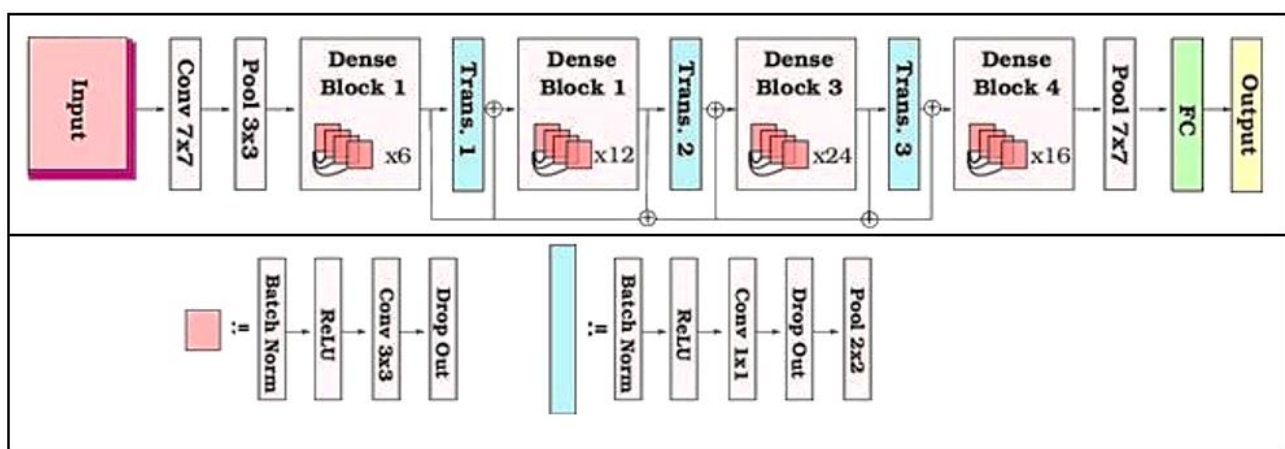

Figure 3. DenseNet architecture. Source (Singh et al., 2021).

DenseNet models are constructed using an alternating pattern of dense and transition pieces. Within a thick block, the feature map dimensions stay fixed to facilitate their concatenation, but their volume

fluctuates. On the other hand, transition blocks perform downsampling between dense blocks using 1 × 1 convolution and 2 × 2 pooling layers. The dense layer basically performs the following activation function to generate output to the next layer using Equation (3).

$$y = activation(dot(x, k) + b) \tag{3}$$

where y is the output, x is the input, k is the kernel, dot is the dot product operation between the x and k, and b is the bias.

The network design contains a single hyperparameter called the growth rate. It regulates the network data capacity of each layer. The following equation is used to calculate the growth rate.

$$f_l = f_0 + k * (l - 1) \tag{4}$$

where the hyperparameter f represents the size of the feature maps or the growth rate of a particular l layer. This parameter limits the number of feature maps added by each layer, thus controlling the quantity of information supplied to the global state by each layer. DenseNets outperformed other state-of-the-art benchmark models in object recognition. It requires fewer parameters and less processing time.

3.4 Resnet152 model

ResNet has been named the winner of the ILSVRC 2015 in image classification, detection and localization, as well as the winner of the MS COCO 2015 in detection and segmentation (Hezam et al., 2021). ResNet-152 is a CNN with 152 layers of depth that was developed by Google (Guo et al., 2019). ResNet-152 initially uses the VGG-19 architecture of a 34-layer plain network, as shown in Figure 4 (Han et al., 2018). By learning residual representation functions rather than learning the signal representation directly, ResNet can build an extremely deep network with up to 152 layers (Furusho et al., 2019; Boulahia et al., 2022).
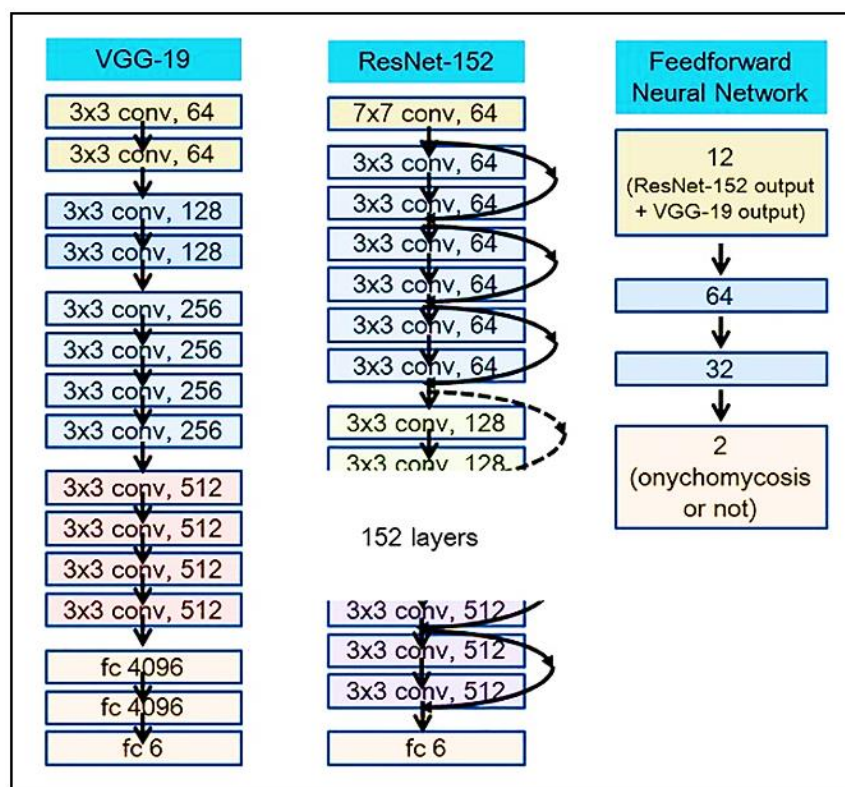

Figure 4. *ResNet architecture. Sources (Tsang, 2018; Han et al., 2018).*

To fit the input from the previous layer to the next layer without changing the input, ResNet provides a residual connection and skip connection (also known as a shortcut connection) (Guo et al., 2019). The

residual connection represents the layers that have the required learning attributes. The residual connection can be mathematically represented as in Equation (5).

$$F(x) = x + G(x) \tag{5}$$

The skip connection represents the layers that do not have the required learning attributes. The ability to skip connections allows ResNet to develop a more flexible network. Adding a skip or shortcut connection to the output after a few weight layers helps overcome the issue of vanishing or exploding gradients (Zhang et al., 2022). The skip operation can be represented as in Equation (6).

$$F(x) = H(x) - x \tag{6}$$

Figure 5 shows the shortcut connection to the output after a few weight layers. In Figure 4, the output $H(x)$ = $F(x) + x$ is obtained. The purpose of the weight layers is to learn a kind of residual mapping.
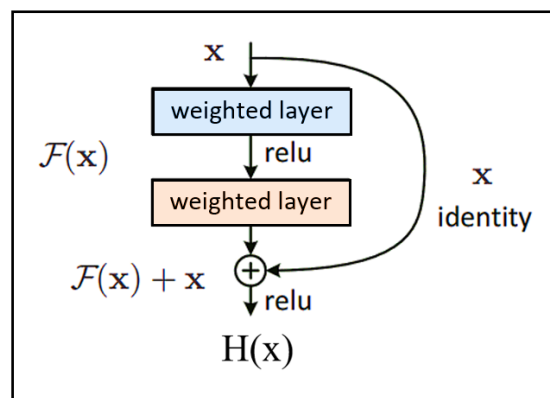

Figure 5. *Residual network building block. Source (Mao et al., 2016).*

3.5 Evaluation metrics

A confusion matrix is defined as a graphical representation of the outcomes of a classification problem prediction. In each class, the number of right and wrong predictions is summarized with count values and broken down further per class member. It demonstrates in many ways the performance of the tested model while making predictions (Abd ElGhany et al., 2021). The accuracy, precision, recall (sensitivity), f1 score and ROC are generated from the confusion matrix of the classification results as standard assessment metrics. Table 2 shows the subsequent metrics equations: T represents true, F represents false, P represents positive, and N represents negative.

Table 2. *Evaluation metrics.*

Metric	Equation
Accuracy	ACC = (TP + TN) / (TP + TN + FP + FN)
Precision	PPV = TP / (TP + FP)
Recall	TPR = TP / (TP + FN)
F1 Score	F1 = 2TP / (2TP + FP + FN)
ROC Score	roc_score = roc_auc_score(y_true, y_predicted)

4   Solution and Results

4.1   Model design and setting

The construction of a viable automated detection model for melanoma lesions requires acquiring an adequate input set of data to ensure effective model execution (Cassidy et al., 2022). The pre-processing of the dataset is straightforward as the dataset is balanced and contains two folders for testing and training. The ResNet152 model and the other two classifiers have the same parameter settings, as shown in Table 3.

Table 3. Parameters settings of DL models.

Parameter	Setting
Input shape	224,224,3
Epochs	40
Optimizer	Adam
Learning rate	0.0001
Beta_1	0.9
Beta_2	0.999
Epsilon	1e-3
Rectifier	ReLU
Activation function	SoftMax
Loss function	Categorical cross-entropy
Metrix	Accuracy
Folds	4
Output	2

The input layer of the ResNet152 model is set to 224 x 224 pixels in width and height, and the output layer is substituted with the SoftMax activation function. The ResNet152 model has autonomous feature extraction capabilities that make it simple to discover the traits that differentiate each form of cancer without having to use additional operators to evaluate them (Boulahia et al., 2022). We use the TL method to train the ResNet152 model rapidly and fine-tune the training parameters. The network is trained using a learning rate of 0.0001 over 40 epochs and a batch size of 32. Four folds are used in the training phase to ensure the best training is provided for the models, as shown in Figure 7. Adam was selected as the optimization method for this network, including Momentum and Root Mean Square Propagation (RMSP) algorithms. The Momentum algorithm uses the exponential weighted average (EWA) of the gradient to accelerate the gradient descent performance. The following equation calculates the aggregates of the gradients.

$$m_t = \beta m_{t-1} + (1-\beta)\left[\frac{\partial L}{\partial w_t}\right] \qquad (7)$$

Where $w_{t+1} = w_t - \alpha m_t$, t is the time, w is the weight, α is the learning rate, ∂L is the loss function derivative, ∂w_t is the derivative of the weight, and β is the moving average, which usually has a constant value of 0.9.

The RMSP algorithm provides an adaptive learning method to improve the performance of the model based on the following equation.

$$w_{t+1} = w_t - \frac{\alpha_t}{(v_t+\epsilon)^{\frac{1}{2}}} * \left[\frac{\partial L}{\partial w_t}\right] \tag{8}$$

Where v_t is the sum of the square of past gradients and ϵ is a small constant, which has a positive value of 10^{-8}.

The model classifies skin cancer according to the two labels Benign and Malignant. After 40 epochs that are repeated for four folds, the model parameters with the best performance are chosen based on the ensemble method. These parameters are used in conjunction with the testing set of images to improve the overall network performance. An early stopping function is added to monitor the validation of the accuracy throughout the 4-fold fitting process to stop the process when there is no progress in the accuracy. The epochs are also set to 40 for each fold in the testing phase. The test results are plotted with the confusion matrix and the ROC curve, as shown in Figure 9.

4.2 Implementation

A deep residual learning skin cancer recognition (ResNetScr) system based on the ResNet152 model is developed in this study. For the implementation of this project, we have used Python and Python libraries such as Keras, Pandas, Scikit-Learn, Gradio and Numpy on the Kaggle platform. The libraries are free and open-source, allowing quick construction of easy-to-use, customized ML and DL models (Abid et al., 2019).

A user interface was also developed to turn the model into an online application, as shown in Figure 6. We embedded the graphical user interface directly into the Python notebook and used shared URLs for those interested in using the system. In the future, the ResNetScr system could be used as a tool to identify related images of skin tumour types.
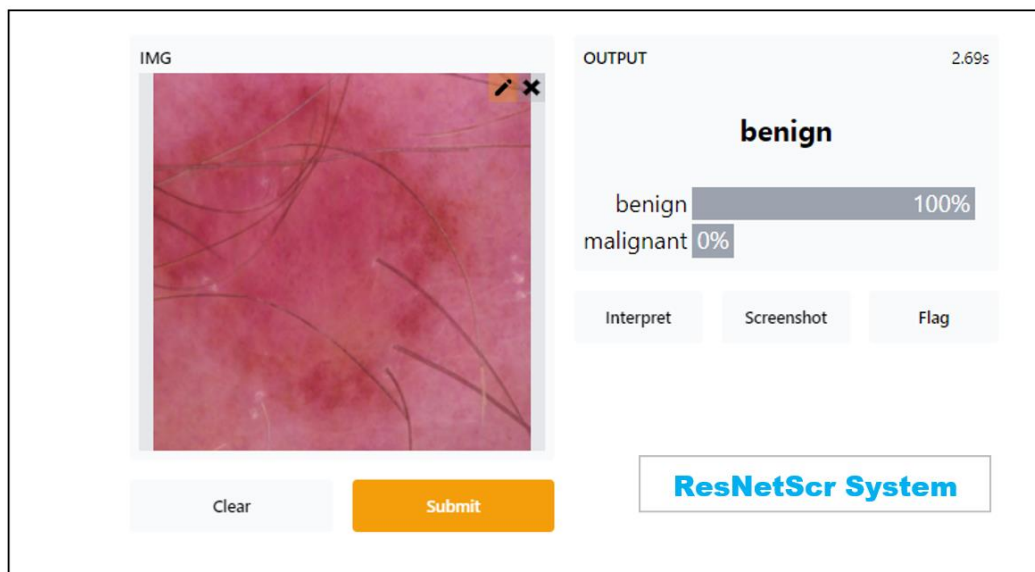

Figure 6. ResNetScr system interface.

4.3 Results and discussion

The results of the three models DenseNet121, ResNet152 and VGG19 are tested on a skin image dataset in a classification experiment. Table 4 shows the results of the three models. We can see from the results that the ResNet152 model outperforms the others by a wide margin and achieves the best performance. It achieves an average accuracy score of 91% during training and 92% during testing. In addition, the model outperformed the other two models in every metric we have examined. The DenseNet121 model obtained the second-best results, and the VGG19 achieved the lowest outcomes in every metric measured.

**Table 4.** *Average test results of DL models.*

Model	Accuracy	Loss	Precision	Recall	f-1 score	ROC
VGG19	0.796	0.434	0.800	0.800	0.800	0.750
DenseNet121	0.900	0.300	0.890	0.890	0.840	0.880
ResNet152	0.922	0.230	0.947	0.914	0.930	0.909

Figure 7 shows the performance of the ResNet152 model over the training folds. More detailed results of the ResNet152 performance during the training phase can be seen in the classification report shown in Table 5.

Table 5. *ResNet152 model training results.*

Classification	Precision	Recall	F1 score	Support
Benign	0.92	0.92	0.92	360
Malignant	0.90	0.90	0.90	300
All classes	0.91	0.91	0.91	660
Macro avg.	0.91	0.91	0.91	660
Weighted avg.	0.91	0.91	0.91	660

Subsequently, Figure 8 shows the confusion matrix for the ResNet152 classifier during the testing phase. The confusion matrix presents the benign and malignant true and false classification results, in which benign has the scores of 341 TP and 19 TN, and malignant has the scores of 268 TN and 32 FN.
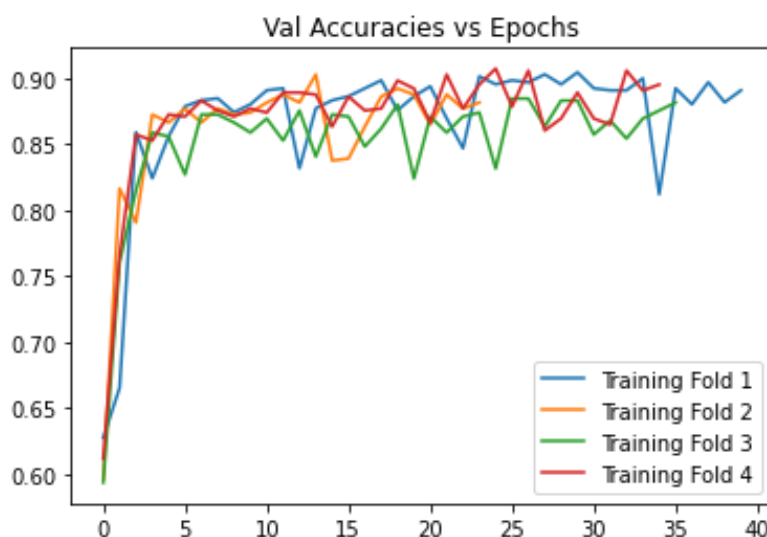
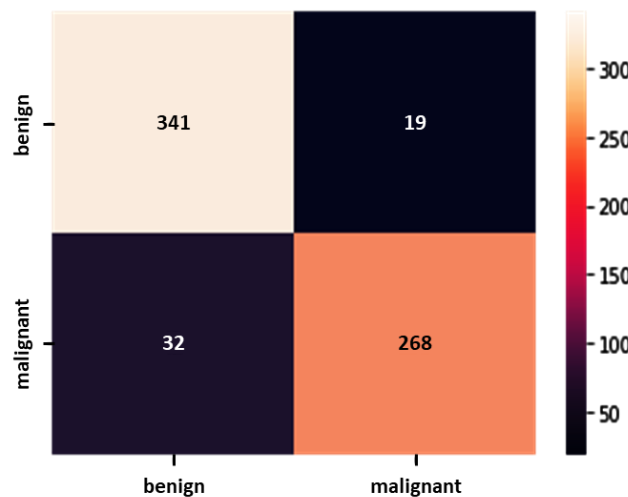**Figure 7.** *ResNet152 training accuracy over epochs for 4 folds.*

Figure 8. ResNet152 confusion matrix.

The ResNet152 model, after the provided improvement, proved to be the best among the other models. Its ability to classify skin cancer is well presented in Figure 9, in which the ResNet152 model obtains an ROC score of 90.09%, as shown in Table 5.
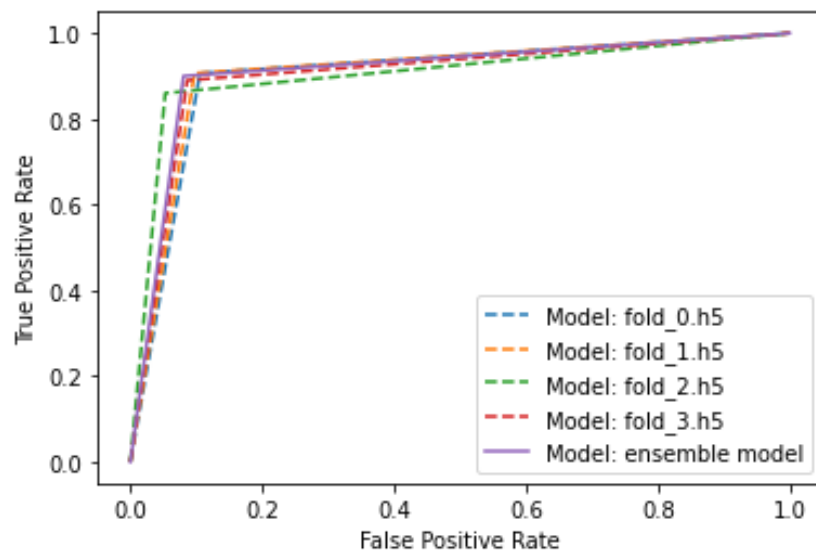

Figure 9. ResNet152 ROC curve.

5 Conclusion

Early diagnosis of skin cancer is an important step for its treatment success. This type of cancer appears first as a discoloured patch or a lump on the skin. In time, it progresses to a tumour. In this paper, we used three CNN DL classification models in an attempt to identify their ability to classify skin cancer images to ease its early diagnosis. The models are DenseNet121, ResNet152 and VGG19. We contributed to improving the ResNet152 model by adding a transfer learning method, optimization functions and training strategy. A set of identical operation and evaluation parameters were applied to all three models during the experimental setting. In the training and testing phases, we used 4-fold cross-validation over 40 epochs in order to acquire more accurate results. As stated in the results, the experiment outcomes reveal that the ResNet152 model outperforms the other two models on every metric evaluated.

The ResNet152 model achieves the best accuracy score of 92% and ROC score of 91%. Subsequently, a deep residual learning skin cancer recognition (ResNetScr) system was implemented based on the

ResNet152 model for online skin cancer recognition. In the future, the ResNetScr system could be used to identify related images of skin tumour types. Moreover, an advanced TL algorithm needs to be considered to pre-train the ResNet152 model in order to acquire more robust results.

Additional Information and Declarations

Conflict of Interests: The authors declare no conflict of interest.

Author Contributions: J.M.A-T.: Conceptualization, Methodology, Software, Data curation, Validation, Writing – Original draft preparation, Writing – Reviewing and Editing. N.T.Y.: Conceptualization, Methodology, Software, Data curation, Validation, Writing – Original draft preparation, Writing – Reviewing and Editing. N.A.M.A.: Conceptualization, Methodology, Software, Data curation, Validation, Writing – Original draft preparation, Writing – Reviewing and Editing. S.M.: Conceptualization, Methodology, Software, Data curation, Validation, Writing – Original draft preparation, Writing – Reviewing and Editing.

Institutional Review Board Statement: Ethical review and approval were waived for this study due to the use of the external and publicly available dataset.

Data Availability: The used external dataset (from the ISIC archive) for this research is available online and has a proper citation in the article.

References

Abd ElGhany, S., Ramadan Ibraheem, M., Alruwaili, M., & Elmogy, M. (2021). Diagnosis of Various Skin Cancer Lesions Based on Fine-Tuned ResNet50 Deep Network. *Computers, Materials & Continua*, 68(1), 117–135. https://doi.org/10.32604/cmc.2021.016102

Abid, A., Abdalla, A., Abid, A., Khan, D., Alfozan, A., & Zou, J. (2019). Gradio: Hassle-Free Sharing and Testing of ML Models in the Wild. *arXiv preprint* arXiv:1906.02569. https://doi.org/10.48550/arXiv.1906.02569

Baig, R., Bibi, M., Hamid, A., Kausar, S., & Khalid, S. (2019). Deep Learning Approaches Towards Skin Lesion Segmentation and Classification from Dermoscopic Images – A Review. *Current Medical Imaging Reviews*, 16(5), 513-533. https://doi.org/10.2174/1573405615666190129120449

Bellu, E., Medici, S., Coradduzza, D., Cruciani, S., Amler, E., & Maioli, M. (2021). Nanomaterials in Skin Regeneration and Rejuvenation. *International Journal of Molecular Sciences*, 22(13), Article 7095. https://doi.org/10.3390/ijms22137095

Boulahia, S. Y., Benatia, M. A., & Bouzar, A. (2021). Att2ResNet: A deep attention-based approach for melanoma skin cancer classification. *International Journal of Imaging Systems and Technology*, 32(2), 476–489. https://doi.org/10.1002/ima.22687

Cassidy, B., Kendrick, C., Brodzicki, A., Jaworek-Korjakowska, J., & Yap, M. H. (2022). Analysis of the ISIC image datasets: Usage, benchmarks and recommendations. *Medical Image Analysis*, 75, Article 102305. https://doi.org/10.1016/j.media.2021.102305

Codella, N., Rotemberg, V., Tschandl, P., Celebi, M. E., Dusza, S., Gutman, D., ... & Halpern, A. (2019). Skin Lesion Analysis Toward Melanoma Detection 2018: A Challenge Hosted by the International Skin Imaging Collaboration (ISIC). *arXiv preprint* arXiv:1902.03368. https://doi.org/10.48550/arXiv.1902.03368

Dildar, M., Akram, S., Irfan, M., Khan, H. U., Ramzan, M., Mahmood, A. R., Alsaiari, S. A., Saeed, A. H. M., Alraddadi, M. O., & Mahnashi, M. H. (2021). Skin Cancer Detection: A Review Using Deep Learning Techniques. *International Journal of Environmental Research and Public Health*, 18(10), Article 5479. https://doi.org/10.3390/ijerph18105479

Fujisawa, Y., Otomo, Y., Ogata, Y., Nakamura, Y., Fujita, R., Ishitsuka, Y., Watanabe, R., Okiyama, N., Ohara, K., & Fujimoto, M. (2018). Deep-learning-based, computer-aided classifier developed with a small dataset of clinical images surpasses board-certified dermatologists in skin tumour diagnosis. *British Journal of Dermatology*, 180(2), 373–381. https://doi.org/10.1111/bjd.16924

Furusho, Y., & Ikeda, K. (2019). Resnet and batch-normalization improve data separability. In *Asian Conference on Machine Learning* (pp. 94-108). PMLR. https://proceedings.mlr.press/v101/furusho19a.html

Guo, Q., Yu, X., & Ruan, G. (2019). LPI radar waveform recognition based on deep convolutional neural network transfer learning. *Symmetry*, 11(4), Article 540. https://doi.org/10.3390/sym11040540

Han, S. S., Park, G. H., Lim, W., Kim, M. S., Na, J. I., Park, I., & Chang, S. E. (2018). Deep neural networks show an equivalent and often superior performance to dermatologists in onychomycosis diagnosis: Automatic construction of onychomycosis datasets by region-based convolutional deep neural network. *PloS One*, 13(1), e0191493. https://doi.org/10.1371/journal.pone.0191493

Hezam, A. A., Mostafa, S. A., Baharum, Z., Alanda, A., & Salikon, M. Z. (2021). Combining Deep Learning Models for Enhancing the Detection of Botnet Attacks in Multiple Sensors Internet of Things Networks. *International Journal on Informatics Visualization*, 5(4), 380–387. https://doi.org/10.30630/joiv.5.4.733

Li, K. M., & Li, E. C. (2018). Skin lesion analysis towards melanoma detection via end-to-end deep learning of convolutional neural networks. *arXiv preprint* arXiv:1807.08332. https://doi.org/10.48550/arXiv.1807.08332

Mao, X. J., Shen, C., & Yang, Y. B. (2016). Image restoration using convolutional auto-encoders with symmetric skip connections. *arXiv preprint* arXiv:1606.08921. https://doi.org/10.48550/arXiv.1606.08921

Pacheco, A. G., Ali, A. R., & Trappenberg, T. (2019). Skin cancer detection based on deep learning and entropy to detect outlier samples. *arXiv preprint* arXiv:1909.04525. https://doi.org/10.48550/arXiv.1909.04525

Pérez, E., Reyes, O., & Ventura, S. (2021). Convolutional neural networks for the automatic diagnosis of melanoma: An extensive experimental study. *Medical Image Analysis*, 67, Article 101858. https://doi.org/10.1016/j.media.2020.101858

Pushpalatha, A., Dharani, P., Dharini, R., & Gowsalya, J. (2021). Skin Cancer Classification Detection using CNN and SVM. *Journal of Physics: Conference Series*, 1916, Article 012148. https://doi.org/10.1088/1742-6596/1916/1/012148

Simonyan, K., & Zisserman, A. (2014). Very deep convolutional networks for large-scale image recognition. *arXiv preprint* arXiv:1409.1556. https://doi.org/10.48550/arXiv.1409.1556

Singh, D., Kumar, V., & Kaur, M. (2021). Densely connected convolutional networks-based COVID-19 screening model. *Applied Intelligence*, 51(5), 3044-3051. https://doi.org/10.1007/s10489-020-02149-6

Tsang, S.-H. (2018). Review: ResNet — Winner of ILSVRC 2015 (Image Classification, Localization, Detection). https://towardsdatascience.com/review-resnet-winner-of-ilsvrc-2015-image-classification-localization-detection-e39402bfa5d8

Tschandl, P., Rosendahl, C., & Kittler, H. (2018). The HAM10000 dataset, a large collection of multi-source dermatoscopic images of common pigmented skin lesions. *Scientific Data*, 5(1), 1–9. https://doi.org/10.1038/sdata.2018.161

Valdés-Morales, K. L., Peralta-Pedrero, M. L., Jurado-Santa Cruz, F., & Morales-Sanchez, M. A. (2020). Diagnostic Accuracy of Dermoscopy of Actinic Keratosis: A Systematic Review. *Dermatology Practical & Conceptual*, 10(4), e20200121. https://doi.org/10.5826/dpc.1004a121

Yu, Z., Ni, D., Chen, S., Qin, J., Li, S., Wang, T., & Lei, B. (2017). Hybrid dermoscopy image classification framework based on deep convolutional neural network and Fisher vector. In *2017 IEEE 14th international symposium on biomedical imaging (ISBI 2017)* (pp. 301–304). IEEE. https://doi.org/10.1109/ISBI.2017.7950524

Zhang, L., Li, H., Zhu, R., & Du, P. (2022). An infrared and visible image fusion algorithm based on ResNet-152. *Multimedia Tools and Applications,* 81(7), 9277–9287. https://doi.org/10.1007/s11042-021-11549-w

Zheng, Y., Yang, C., & Merkulov, A. (2018). Breast cancer screening using convolutional neural network and follow-up digital mammography. In *Proceedings Volume 10669, Computational Imaging III* (paper 1066905). SPIE. https://doi.org/10.1117/12.2304564

Zhu, W., Xie, L., Han, J., & Guo, X. (2020). The Application of Deep Learning in Cancer Prognosis Prediction. *Cancers*, 12(3), Article 603. https://doi.org/10.3390/cancers12030603